BILINGUAL PUBLISHING GROUP

Journal of Environmental & Earth Sciences

https://journals.bilpubgroup.com/index.php/jees

REVIEW

Flood Mapping Methodologies in Google Earth Engine Using Optical and Radar Data: A Comparative Study

Yassine Loukili [*] **, *Younes Lakhrissi*** **, *Safae Elhaj Ben Ali***

SIGER Laboratory, Sidi Mohamed Ben Abdellah University, Fez 30000, Morocco

ABSTRACT

Floods are among the most severe and frequent natural disasters, impacting numerous countries worldwide. This study investigates flood mapping methodologies utilizing Google Earth Engine (GEE) with Sentinel-1, Sentinel-2, and Landsat data, focusing on the January 2021 Tetouan flood in Morocco. Three approaches were assessed: Sentinel-1 thresholding and NDWI (Normalized Difference Water Index) methods applied to Sentinel-2 and Landsat imagery. The analysis revealed flooded areas of 891 hectares (Sentinel-1), 814 hectares (Sentinel-2), and 1237 hectares (Landsat), validated against ArcGIS (Geographic Information System) results estimating 900 hectares. Sentinel-1 demonstrated superior accuracy with only a 9-hectare deviation and proved effective under cloudy conditions. Sentinel-2 provided a balance between spatial resolution and error levels, with moderate commission and omission errors. Landsat detected the largest flood extent but exhibited a slight overestimation. The study emphasizes the advantages of GEE's cloud-based platform, which significantly reduced processing time, facilitating rapid flood extent mapping. This scalability and efficiency make GEE an invaluable tool for disaster management. The results underline the potential of these methodologies for accurate and timely flood monitoring, enabling informed decision-making in resilience planning and emergency response. Such advancements are critical for mitigating the impacts of flooding and supporting sustainable disaster management strategies in vulnerable regions worldwide.

Keywords: Flood; Google Earth Engine; Sentinel-1; Sentinel-2; Landsat

*CORRESPONDING AUTHOR:

Yassine Loukili, SIGER Laboratory, Sidi Mohamed Ben Abdellah University, Fez 30000, Morocco; Email: yassine.loukili1@usmba.ac.ma

ARTICLE INFO

Received: 1 October 2024 | Revised: 29 October 2024 | Accepted: 8 November 2024 | Published Online: 24 December 2024
DOI: https://doi.org/10.30564/jees.v7i1.7397

CITATION

Loukili, Y., Lakhrissi, Y., Elhaj Ben Ali, S., 2024. Flood Mapping Methodologies in Google Earth Engine Using Optical and Radar Data: A Comparative Study. Journal of Environmental & Earth Sciences. 7(1): 363–380. DOI: https://doi.org/10.30564/jees.v7i1.7397

1. Introduction

Floods are among the most frequent and destructive natural disasters worldwide, posing significant risks to lives, infrastructure, and economies. This risk is heightened in regions like Morocco, where mountainous terrain, intense precipitation, and rapid urbanization contribute to severe flooding, particularly in vulnerable areas such as the Tanger-Tetouan-Al Hoceima region. The January 2021 Tetouan flood event underscored the need for effective, timely flood mapping to support disaster management and resilience planning.

Field surveys for flooded areas are challenging and impractical for extensive regions, making satellite observation a realistic choice for near-real-time flood monitoring. Numerous flood mapping techniques have been developed in recent years, utilizing various data sources, including satellite, aerial, and in-situ data. Satellites such as Sentinel-1, Sentinel-2, and Landsat, currently in orbit, capture a wide range of data, allowing for multi-temporal, multi-sensor, and multi-scale analyses[1]. These satellites offer unique capabilities for flood monitoring due to their high spatial and temporal resolution, global coverage, and free availability[2]. Combined with the Google Earth Engine cloud computing platform, which provides a wide array of tools and algorithms for flood mapping, a powerful and flexible solution for processing and analyzing these Geospatial Big Data is available[3]. The GEE platform has been instrumental in addressing urgent environmental issues such as drought and deforestation[4], natural disasters[5], climate and environmental problems, and food security[6].

Researchers worldwide have conducted extensive research on flood mapping from optical and radar images. Sentinel-1, with its Synthetic Aperture Radar (SAR) technology, has proven effective in detecting flood areas with approximately 90% accuracy, as SAR can capture high-resolution images regardless of cloud cover or lighting conditions[2, 7–9]. Sentinel-2, with its 10-meter multispectral resolution, allows for detailed flood mapping using indices such as NDWI, achieving an overall accuracy rate of 85−90% under clear skies[1, 10]. Landsat, though less frequent in revisits, has been effective for historical flood analysis with spatial resolutions up to 30 meters and accuracy rates of around 80−85% in cloud-free conditions[11–13].

This study builds upon the strengths of Sentinel-1, Sentinel-2, and Landsat in flood detection by utilizing GEE for enhanced processing speed and scalability. By implementing thresholding on Sentinel-1, NDWI on Sentinel-2, and NDWI on Landsat, the presented methodologies aim to improve both the accuracy and response time of flood mapping. These approaches were tested during the Tetouan flood event, providing critical flood extent data that aligns with ArcGIS benchmarks, thus supporting the reliability of each method for rapid flood assessment.

The article is structured as follows: Section 1 provides a general introduction. Section 2 presents the study area and data used. Section 3 outlines the flood mapping methodology for each data type. Section 4 presents results and compares different methodologies. Finally, Section 5 discusses results and implications, providing a detailed synthesis.

The findings of this study will enhance the accuracy and efficiency of flood mapping, contributing to better disaster management and resilience planning.

2. Materials

2.1. Study Area

The study area covers approximately 50 km², situated in northern Morocco, precisely within the Tetouan Province and M'diq-Fnideq Prefecture (see **Figure 1**).

Figure 1. Study area—Tetouan city.

With a population exceeding 3.9 million inhabitants in 2022, the Tanger-Tétouan-Al Hoceima region is among Morocco's most densely populated areas. In terms of hydraulic resources, the region is crisscrossed by significant water-

courses and experiences high levels of rainfall, endowing it with a considerable renewable water potential estimated at around 4 billion m³ per year[14].

This area has suffered several damages in the past due to flooding associated with its geographic characteristics. Extreme hydrological events like the December 1998 flood, with a peak flow reaching 1927 m³ s–1, and the December 26, 2000 flood, with a peak flow of 2674 m³ s–1, resulted in significant human losses: 8 deaths and 2 missing persons (according to local authorities). The January 17, 2006 floods caused substantial material damages estimated at 83 million Dirhams, submerging 2400 ha[15]. The most recent flood occurred in January 2021, when Tetouan city experienced heavy rainfall and thunderstorms, severely affecting infrastructure and roads. Approximately 9 km² of land were potentially submerged by water[16].

2.1.1. Terrain

The Martil river basin consists of two zones[17]:

- The upstream zone comprises Paleozoic terrains located at the western end of the basin, with ridge heights not exceeding 400 meters.
- The downstream zone corresponds to the Martil river plain, which is a flood-prone area.

The Martil river basin is one of the Mediterranean basins characterized by a relatively large area and varied morphology, with a fairly dense hydrographic network. Its surface area is 1126 km², with a perimeter of 183 km. This watershed is subdivided into 8 significant sub-basins[15]. Significant drops occur due to the proximity of the mountains to the sea. Three-quarters of the river's tributaries pass through the Tétouan city gorge, with the main river receiving waters from three major tributaries: Mhajrat, Khemis, and Chekkoûr, depicted in **Figure 2**, before flowing through Tetouan city and emptying into the Mediterranean in the southern part of Martil city, with a minimum flow rate during low-water periods of 0.23 $m^3 s^{-1}$ [15].

2.1.2. Climate

The climate of the study area is characterized by two distinct seasons: the first, humid and cool, extends from October to April, while the second, sub-humid and hot, begins in May and lasts until the end of September. Precipitation varies in height, intensity, and geographical distribution, with alternating long periods of drought followed by torrential and irregular rainfall. **Figure 3** displays the precipitation averages of the study area from 2020 to 2023.

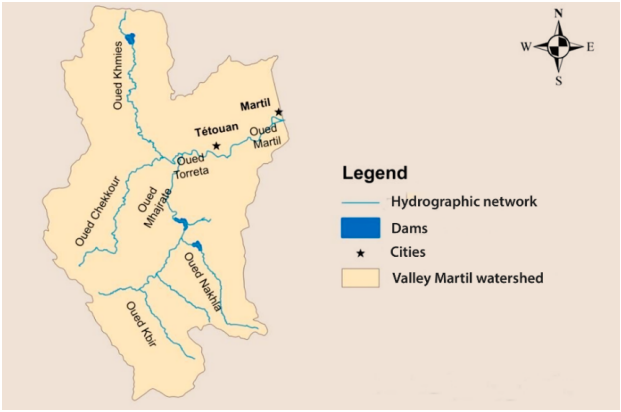

Figure 2. Hydrographic network map of Martil river basin[15].

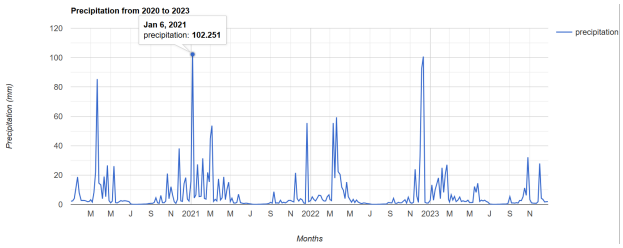

Figure 3. Precipitation averages of the study area from 2020 to 2023 (CHIRPS precipitation data from the Climate Hazards Group).

This analysis of the study area underscores the immense need for flood maps, which can aid in post-disaster management activities and resilient disaster planning.

2.2. Materials

For flood mapping, three types of data available within the Google Earth Engine platform will be utilized: Sentinel-1, Sentinel-2, and Landsat.

2.2.1. Sentinel-1 Data

Sentinel-1 is a satellite from the European Union's Copernicus monitoring mission, considered among the first in a series of Earth imaging satellites. Sentinel-1A was launched in April 2014, followed by Sentinel-1B in April 2016[12]. It is equipped with a SAR sensor capable of capturing images of the Earth's surface at any time, even in challenging weather conditions or low light. Sentinel-1 is employed for monitoring coastal areas, maritime zones, ice zones, deforested areas, and areas at risk of natural disasters.

Sentinel-1 satellite data is operationally acquired in four imaging modes: Strip Map (SM), Interferometric Wide Swath (IW), Extra-Wide Swath (EW), and Wave Swath (WV), each with different acquisition configurations [16]. The Sentinel-1 can transmit signals in horizontal (H) or vertical (V) polarization and receive in both H and V polarizations (see **Figure 4**).

Each of the two Sentinel-1 satellites orbits the globe every 12 days, enabling a potential joint revisit frequency of 6 days over the equator and a revisit frequency of 3 days when considering both ascending and descending orbits [12] (see **Figure 5**).

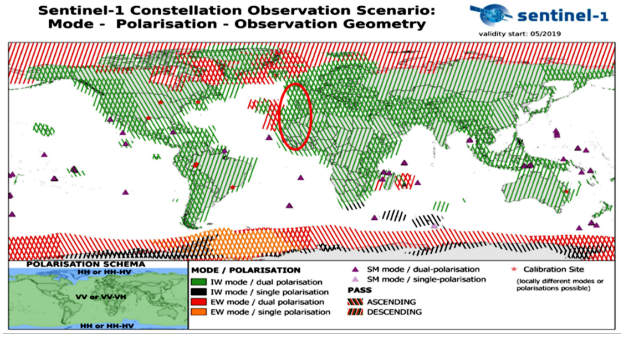

Figure 4. Areas mapped with Sentinel-1, showing high level information (mode, polarisation, cycle validity period) [18].

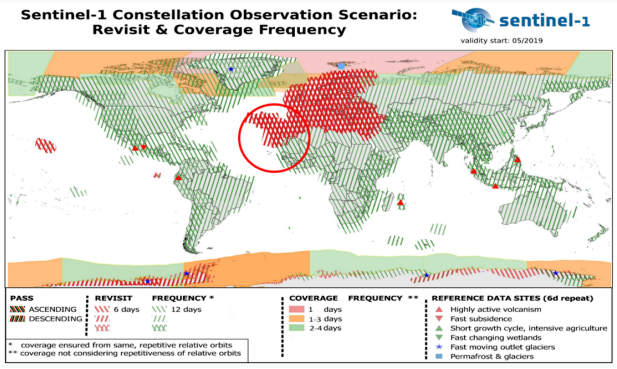

Figure 5. Revisit and coverage frequency of the Sentinel-1 constellation, showing which areas are mainly covered with descending or ascending imagery [18].

The IW mode was utilized in our study as it is the primary mode for acquiring land surface imagery that meets contemporary service requirements with long-term archives [19] (see **Figure 4**). Furthermore, the IW mode of Sentinel-1 is employed to monitor floods as it can detect water height variations in flood-prone areas using interferometric radar techniques. This allows for real-time flood tracking and prediction of potentially affected areas. Additionally, the IW mode of Sentinel-1 can operate even in low-visibility conditions, such as clouds and rain, making it particularly useful for monitoring floods in climatically unstable areas [19].

Moreover, SAR polarization is a key factor in flood detection. Previous studies [20, 21] have shown that horizontally polarized (HH) images are considered more suitable for flood detection than vertically polarized (VV) or cross-polarized (VH) images. However, for this study, the available image during the flood had a VV and VH intensity polarization. Anusha and Bharathi [22] and Psomiadis [23] reported that VV polarization had potential in flood mapping because the co-polarized VV band has stronger backscatter intensities than the cross-polarized VH band. In our case, VH polarization was preferred over VV polarization as it was more suitable for our study area. In total, from a collection of 850 images taken for the study area since 2014, four scenes were selected to enable flood monitoring during the period from January 6 to January 15, 2021: two scenes before the flood and two scenes after the flood (see **Figure 6**).

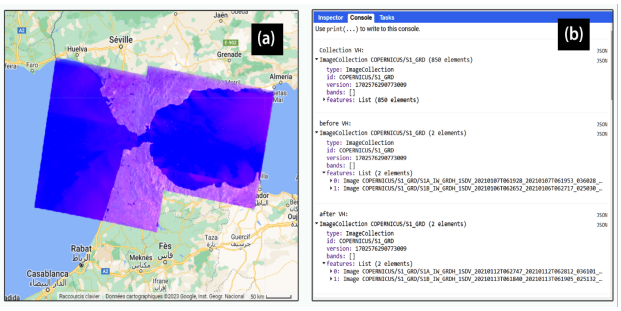

Figure 6. (**a**) Selected images before and after the flood and (**b**) Console sentinel-1 script [24].

The Sentinel-1 Ground Range Detected (GRD) images obtained from the GEE platform are already preprocessed [25], with a pixel size of 10 × 10 m and an image band width equal to 250 km. As Sentinel-1's orbital information is accurate, the terrain-corrected SAR images also have subpixel geolocation accuracy [26]. The specifications of the SAR images used in our work are provided in **Table 1**.

2.2.2. Sentinel-2 Data

With a mass of 1,140 kg, the European observation satellite Sentinel-2A was launched on June 23, 2015, from Kourou aboard a Vega rocket. Its twin, Sentinel-2B, joined it on the same orbit at an altitude of 786 km on March 6, 2017. Publicly accessible, the Sentinel-2A (Sentinel-2 MSI: MultiSpectral Instrument, Level-1C) [27] and Sentinel-2B (Har-

Table 1. Image dataset Sentinel-1.

Satellite/Sensor	Image Captured	Mode	Acquisition Date	Polarisation	Swath Width	Spatial Resolution	Size in Gb
Sentinel-1A	Before flood	IW	06/01/2021	VH	250 km	10 × 10 m	4.0411
Sentinel-1A	Before flood	IW	07/01/2021	VH	250 km	10 × 10 m	4.0338
Sentinel-1A	After flood	IW	12/01/2021	VH	250 km	10 × 10 m	4.0269
Sentinel-1A	After flood	IW	13/01/2021	VH	250 km	10 × 10 m	4.0312

monized Sentinel-2 MSI: MultiSpectral Instrument, Level-2A)[27] satellite data from the European Space Agency (ESA) are capable of monitoring conditions on the Earth's surface. The revisit time is 10 days with one satellite and 5 days with two satellites. Its spatial resolution is 10 m (bands: 2, 3, 4, and 8), 20 m (bands: 5, 6, 7, 8a, 11, and 12), and 60 m (bands: 1, 9, and 10), and it can provide images with a ground width of 290 km[28].

These satellites are used to support a variety of services and applications offered by Copernicus, including land management, agriculture, forestry, disaster monitoring, humanitarian relief operations, risk mapping, and security issues[29].

In this study, bands 3 and 8 of Sentinel-2-L2A satellite data were used for flood mapping. From a collection of 949 images taken for the study area since 2017, we selected six images during the period from January 1 to January 18, 2021: four before the flood and two after the flood (see **Figure 7**).

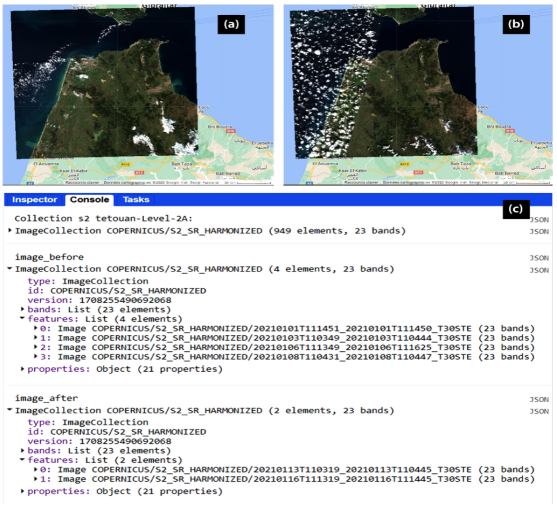

Figure 7. (**a**) Before image true color, (**b**) After image true color, and (**c**) Console Sentinel-2 script[30].

The details of the Sentinel-2 images used to prepare the flood map of the study area are presented in **Table 2**.

Table 2. Images dataset Sentinel-2.

Satellite	Image Captured	Acquisition Date	Band Name	Swath Width	Spatial Resolution	Size in Gb
Sentinel-2 Level 2A	Before flood	01/01/2021	Band 2, Band 3	290 km	10 × 10 m	1.6005
Sentinel-2 Level 2A	Before flood	03/01/2021	Band 2, Band 3	290 km	10 × 10 m	1.6096
Sentinel-2 Level 2A	Before flood	06/01/2021	Band 2, Band 3	290 km	10 × 10 m	1.6099
Sentinel-2 Level 2A	Before flood	08/01/2021	Band 2, Band 3	290 km	10 × 10 m	0.6028
Sentinel-2 Level 2A	After flood	13/01/2021	Band 2, Band 3	290 km	10 × 10 m	0.9246
Sentinel-2 Level 2A	After flood	16/01/2021	Band 2, Band 3	290 km	10 × 10 m	1.4628

2.2.3. Landsat Data

The Landsat missions currently comprise eight operational Earth observation satellites equipped with remote sensors to collect data and images of our planet as part of the United States Geological Survey (USGS) National Land Imaging (NLI) program[31]. Since the launch of Landsat 1 in 1972, the Landsat mission has provided the longest continuous record of the Earth's surface from space. From Landsat 4 onwards, each of the satellites has captured images of the Earth's surface with an optical resolution of 30 meters, approximately once every two weeks, using multispectral and thermal instruments[32]. Thanks to the open data policies of USGS and NASA, datasets from Landsat 4 (1982–1993), Landsat 5 (1982–1993), Landsat 7 (1999–2021), and Landsat 8 (2013–2021) are available free of charge as part of the Google Public Cloud Data program. They can be accessed by anyone through the Google Cloud platform[32].

In this study, Landsat 7 and Landsat 8 satellites were used, which are Earth observation satellites utilized for mapping, environmental monitoring, and other applications related to observing the Earth's surface. The complete orbital cycle of Landsat 7 and 8 is 16 days. From a collection of 388 Landsat 7 images and 239 Landsat 8 images taken for the study area, we selected two images during the period from

January 1 to January 15, 2021: one before the flood and the other after the flood (see **Figure 8**).

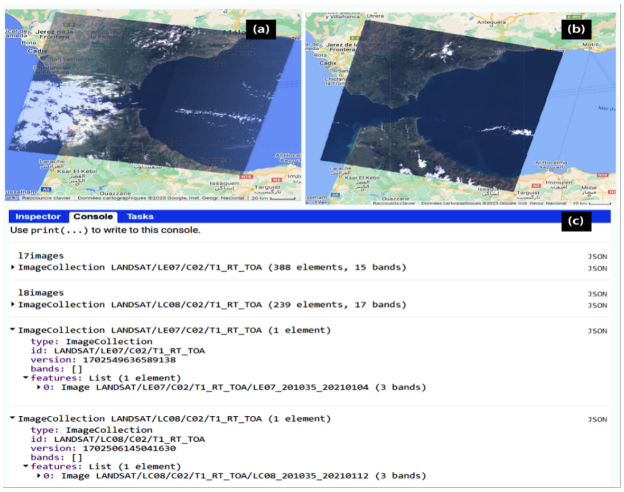

Figure 8. (**a**) True-color composite Landsat 7, (**b**) true-color composite Landsat 8, and (**c**) Console Landsat script[33].

The Landsat images obtained from the GEE platform are already preprocessed and calibrated with a pixel size of 30 × 30 meters[13]. **Table 3** shows the characteristics of the Landsat images used.

3. Methods

In this study, we employed a three-step geospatial analysis workflow to map flood extents using Sentinel-1, Sentinel-2, and Landsat data within the Google Earth Engine (GEE) platform. Each data source was processed independently through a structured methodology, tailored to the unique characteristics of optical and radar data. The workflow began with data acquisition and pre-processing, where images were filtered by acquisition date and atmospheric or radar-specific conditions. This ensured that only images relevant to the flood event in January 2021 were selected, minimizing noise and maximizing detection accuracy.

Next, each data source underwent image analysis to detect flooded areas. For Sentinel-1, thresholding was applied to detect changes in backscatter intensity before and after the flood, highlighting inundated areas. Sentinel-2 and Landsat images were processed using the Normalized Difference Water Index (NDWI), allowing for water detection based on spectral differences in visible and infrared bands. Finally, a validation process was conducted by comparing each flood extent map with results obtained from ArcGIS analysis.

Table 3. Images dataset Landsat.

Satellite	Image Captured	Acquisition Date	Band Name	Spatial Resolution	Size in Gb
Landsat 7	Before flood	04/01/2021	Band 2, Band 3	30 × 30 m	1.6005
Landsat 8	After flood	12/01/2021	Band 2, Band 3	30 × 30 m	1.6096

3.1. Flood Detection Method with Sentinel-1 Data

The Sentinel-1 data required for this study comes from the "COPERNICUS/S1_GRD" dataset provided by the GEE cloud platform, as previously explained. GEE can execute multiple tasks flawlessly, from data retrieval to flood mapping, as it operates on a parallel processing architecture[26].

The methodology followed involves detecting flooded and non-flooded pixels by calculating the difference between images before and after the event to generate a flood extent map for assessing affected areas. The flood mapping processing chain steps have been divided into five modules, namely:

3.1.1. Retrieval of Sentinel-1 Data

A collection of images of the study area used for flood mapping is directly extracted from the Sentinel-1 GEE data catalog[34] to the GEE processing platform using the Earth Engine ee.FeatureCollection() operator.

3.1.2. Metadata Filtering

- Selection of time period and sensor parameters

During this step, a filter is created to narrow down the data volume based on the work objective as the Sentinel-1 image collection extracted from the previous step contains vast information about each image such as data acquisition mode, acquisition time, satellite pass, polarization, etc. Thus, all Sentinel-1 images will be filtered with a descending pass (DESCENDING), wide interferometric mode (IW), and polarization parameters (VH) using the Earth Engine filterMetadata() operator. Additionally, the filterDate() operator will be used by setting the start and end dates to retrieve only images before and after the flood event. Thus, metadata and

spatial filtering play a crucial role in limiting data volume and processing time.

- Smoothing filter

A smoothing filter is applied to the selected images to smooth pixel values[35]. This filter is used to reduce noise or undesirable variations in the data, which can improve readability and interpretation of results. The Earth Engine focal_mean. (SMOOTHING_RADIUS, "circle", "meters") function applies a spatial mean filter with a smoothing radius and circular shape. The smoothing should be strong enough to reduce noise but not so strong as to remove important details. The value (SMOOTHING_RADIUS = 50) was chosen after several tests and proved to be suitable for smoothing small irregularities while preserving larger features. It can be adjusted and optimized based on project specifics and desired results.

3.1.3. Detection of Flooded Pixels

- Calculation of the difference

Here we will use a simple and direct approach for change detection. The mosaic after flooding is divided by the mosaic before flooding using the divide() function. By using pixel-wise division, each pixel in the afterVH image is divided by the corresponding pixel in the beforeVH image. The resulting output is a raster layer showing the degree of change per pixel. This relative difference is useful for detecting significant changes that occurred between the two periods. High values (bright pixels) indicate significant change, while low values (dark pixels) indicate little change. It can highlight areas where radar backscatter has increased (e.g., due to water) or decreased (e.g., due to changes in soil or vegetation). Subsequently, this relative difference is used for thresholding to identify potentially flooded areas in the script.

- Thresholding the difference

Now we will create a binary mask based on the relative difference between images before and after flooding obtained earlier using the selfMask() function that masks the original image using the provided boolean values. This mask highlights areas where the radar backscatter difference exceeds a fixed threshold (DIFF_UPPER_THRESHOLD). This means that only pixels above the threshold will be visible in the resulting image, and others will be masked. The predefined threshold of 1.25 is applied by assigning 1 to all values above 1.25 and 0 to all values below 1.25. Pixels with values above the threshold are considered flooded, and the binary raster layer created by this process will show the potential extent of flooding. The threshold of 1.25 was chosen through trials using the GEE Inspector panel and could be adjusted. These highlighted areas will be used to detect and visualize potentially flooded areas in the next step of the script (see **Figure 9**).

Figure 9. Choice of threshold for identifying flooded areas with Sentinel-1 data.

3.1.4. Refining the Flood Extent Layer

Several additional datasets are used to eliminate false positives in the flood extent layer:

- Calculate pixel connectivity and remove isolated pixels

A connected pixel is a pixel that is adjacent to at least one other change pixel. The connectedPixelCount() function is used to calculate the number of connected pixels. Only change pixels with 8 or more connected pixels will be kept. This operation reduces noise in the flood extent product. The chosen value of 8 has a relationship with the 10 m resolution of Sentinel-1. The 10 m resolution means that each pixel in the image represents a 10 m × 10 m area on the ground. Therefore, a change pixel with 8 or more connected pixels must represent a change area of at least 80 m × 80 m. This size is generally considered large enough to exclude changes due to noise. Indeed, noise is typically limited to areas smaller than 80 m × 80 m[36].

- Remove misclassified pixels in areas where the slope is higher than the average slope

Another refinement level is applied to remove areas with a slope higher than the average slope as they are con-

sidered steep where water would flow away from them and could not be flooded. For this purpose, a Digital Elevation Model (DEM), based on Shuttle Radar Topography Mission (SRTM) data with a resolution of 30 m[1], extracted from archived data of the USGS, is used. The ee.Terrain.slope(srtm) and ee.Algorithms.Terrain(srtm) functions are used to calculate the average slope (average slope = 3.75%) of the study area and exclude resulting flooded change pixels with a slope higher than 4%.

- Remove misclassified pixels in areas where there is permanently free water

To clean classification errors due to permanent water, the Copernicus Global Land Service (CGLS), which provides a global map of land cover at a spatial resolution of 100 m, will be used[37]. In this map, regions of pixels with a class value of 80 (inland water bodies) and a class value of 200 (ocean) will be identified, which have been detected as flooded pixels, and removed.

3.1.5. Calculation of Flood Extent Area

To calculate the flood extent area, a new raster layer is created by multiplying the thresholded image by the area in m^2 of each flooded pixel, using the multiply(ee.Image.pixelArea()) function. By summing all the pixels, information about the area is derived and converted to hectares via the reduceRegion() and getNumber() functions.

Figure 10 illustrates the flowchart of the proposed methodology for rapid flood mapping using Sentinel-1 and GEE.

3.2. Flood Detection Method with Sentinel-2 Data

Sentinel-2-L2A images are corrected for atmospheric effects. L2A data are preferred for applications requiring precise atmospheric correction, such as water quality monitoring, soil mapping, natural resource management, and environmental monitoring[38]. The procedural approach adopted for Sentinel-2-L2A data involves extracting the flood area using the Normalized Difference Water Index (NDWI) from the Sentinel-2 satellite via the GEE environment. Numerous studies have demonstrated that NDWI is highly suitable for extracting water bodies[39, 40]. This approach can be summarized as follows.

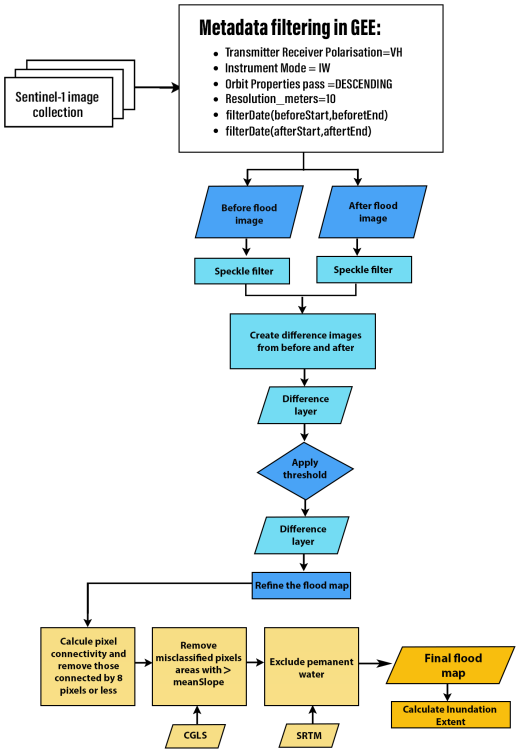

Figure 10. Flowchart of the proposed methodology for flood mapping using Sentinel-1 and GEE.

3.2.1. Definition of Study Area

A collection of images of the study area used for flood mapping is directly extracted from the Sentinel-2 data catalog[27] to the GEE processing platform using the Earth Engine ee.FeatureCollection() operator.

3.2.2. Filtering Images for Pre- and Post-Flooding Periods

Sentinel-2-L2A images are first filtered by date to obtain images for two distinct periods of the event:

- Before period: From January 1st to January 11th, 2021.
- After period: From January 12th to January 18th, 2021.

Then, within each period, the images are sorted by the "CLOUDY_PIXEL_PERCENTAGE" property in descending order to select images with the least cloud cover. Finally, the selected images are merged into a single composite image using the mosaic() function.

3.2.3. Calculation of NDWI

The NDWI is a frequently used index for detecting the presence of water in satellite images. It is calculated for the pre and post-flooding periods from band 3 (B3) and band 8

(B8) of the Sentinel-2-L2A images using the normalizedDifference() function, which subtracts band B3 from band B8 and divides by their sum:

$$\mathbf{NDWI} = (B8 - B3)/(B8 + B3).$$

Band 3's red reflection is sensitive to chlorophyll content in vegetation. Healthy vegetation reflects more red light than near-infrared. Band 8's near-infrared reflection is sensitive to surface moisture. Water reflects more near-infrared light than red. Therefore, the difference between red and near-infrared reflection indices is an indicator of water presence.

3.2.4. Identification of Flooded Areas

Here, the difference between NDWI indices from pre and post-flooding periods is calculated using the subtract() function. The diff.gt(DIFF_THRESHOLD) function creates a binary image (0 or 1) where pixels with an NDWI difference greater than the "DIFF_THRESHOLD" threshold are considered flooded. The threshold value of 0.1 used in this code was chosen based on the desired sensitivity of flooded area detection using the NDWI difference map and GEE's Inspector panel (see **Figure 11**).

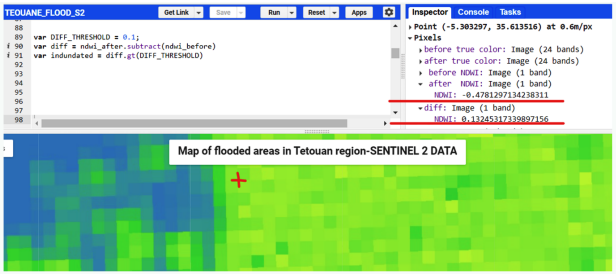

Figure 11. Threshold selection for flood zone identification using NDWI Sentinel-2.

A higher threshold value (e.g., 0.2 or 0.3) will detect larger flooded areas but may also generate false positives, i.e., detect areas as flooded when they are not. A lower threshold value (e.g., 0.05 or 0.01) will detect smaller flooded areas but may also generate false negatives, i.e., not detect flooded areas when they are. The threshold of 0.1 is a good compromise between sensitivity and accuracy. It detects most flooded areas while reducing the risk of false positives.

3.2.5. Calculation of Flooded Area

The flooded area is calculated by multiplying the area of flooded pixels by the area of each pixel using the multiply(ee.Image.pixelArea()) function. Then, the sum of the flooded area is calculated for the area of interest and converted to hectares using the reduceRegion() and getNumber() functions. **Figure 12** illustrates the flowchart of the proposed methodology for rapid flood mapping using Sentinel-2 and GEE.

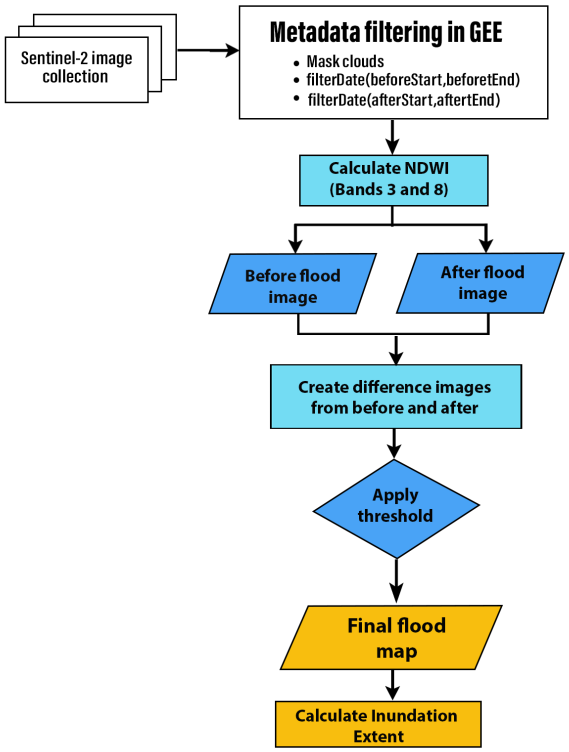

Figure 12. Flowchart of the proposed methodology for rapid flood mapping using Sentinel-2 and GEE.

3.3. Flood Detection Method with Landsat Data

To extract water masses from different Landsat optical images we will use the NDWI index. The main steps to identify flooded areas based on Landsat data are as follows:

3.3.1. Data Loading and Study Area Definition

Firstly, using the ee.FeatureCollection() function, a collection of geometric entities representing the area of interest is loaded. Then, the filterDate() function filters Landsat 7 and Landsat 8 images by date to retain only those taken during the period from January 1st to January 15th, 2021.

3.3.2. Cloud Masking

The cloudfunction() function is used to mask clouds in the images based on the cloud probability score. It calculates

a cloudiness score using the ee.Algorithms.Landsat.simpleCloudScore() function. Then, it creates a cloud mask by selecting pixels with a cloudiness score above a defined threshold. This threshold is used to decide which pixels are considered cloud-covered and should therefore be masked.

3.3.3. Band Selection and NDWI Calculation

The NDWI Index is calculated for each image from the appropriate bands B2 (green), B4 (near-infrared) for Landsat 7 and B3 (green), B5 (near-infrared) for Landsat 8 using the normalizedDifference() function. Bands 2 and 4 of Landsat 7 and bands 3 and 5 of Landsat 8 are chosen to calculate the NDWI because they respectively measure visible light reflection and near-infrared reflection. By using bands 2 and 4 of Landsat 7 or bands 3 and 5 of Landsat 8, water can be effectively distinguished from other surfaces. The NDWI is calculated by subtracting green band reflectance from near-infrared band reflectance. High NDWI values indicate water presence, while low values indicate other surfaces:

NDWI = (Green band − Near-infrared band)/(Green band + Near-infrared band)

3.3.4. Data Fusion and Flooded Area Detection

The Landsat 7 and Landsat 8 image collections are merged into a single collection using the ee.ImageCollection() function. Also, the 10th and 90th percentiles of NDWI are calculated to define "before" and "after" flood conditions using the reduce(ee.Reducer.percentile) function. This means that 10% of pixels will have an NDWI value less than or equal to the pre-flood value and 90% of pixels will have an NDWI value less than or equal to the post-flood value. The 10th percentile is chosen here to represent a reference value for non-flooded water, as it generally corresponds to permanent or semi-permanent water areas. Conversely, the 90th percentile is chosen to represent a potentially higher value related to flooded areas, as floods tend to increase NDWI value in previously non-flooded areas. A difference threshold (DIFF_THRESHOLD) is defined to distinguish flooded from non-flooded areas. The difference between NDWI values of "before" and "after" events is calculated using the subtract() function. An NDWI difference greater than the threshold is considered an indication that the area has experienced flooding.

The threshold of 0.11 used in this code was chosen based on the desired sensitivity of flooded area detection using the NDWI difference map and GEE's Inspector panel (see **Figure 13**).

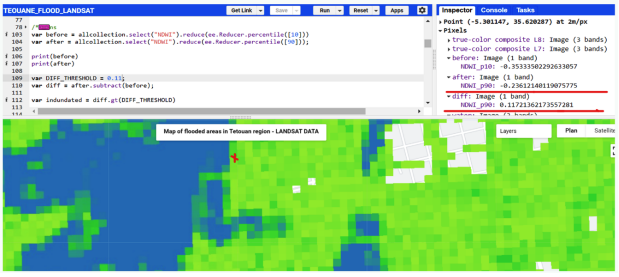

Figure 13. Threshold selection for flood zone identification using NDWI Landsat.

3.3.5. Calculation of Flooded Area

The flooded area is calculated by multiplying the area of flooded pixels by the area of each pixel using the multiply(ee.Image.pixelArea()) function. Then, the sum of the flooded area is calculated for the area of interest and converted to hectares using the reduceRegion() and getNumber() functions.

Figure 14 illustrates the flowchart of the proposed methodology for rapid flood mapping using Landsat and GEE.

3.4. Validation Approach of Different Methods

To validate the accuracy of the flood extent maps generated using Sentinel-1, Sentinel-2, and Landsat data on Google Earth Engine (GEE), we used results from ArcGIS as a benchmark. The flood map (Map produced by UNITAR/UNOSAT[16]) created in ArcGIS was developed using high-resolution data and precise spatial analysis tools, offering a reliable reference for comparison (Satellite data: Pleiades, Resolution: 50 cm[16]). In the analyzed area, which is approximately 50 km^2 , a total of 9 km^2 of land is potentially submerged by water[16].

The comparison process involved overlaying the flood extent maps from GEE onto the ArcGIS-generated map to identify areas of agreement and discrepancy. For each method (Sentinel-1 thresholding, Sentinel-2 NDWI, and Landsat NDWI), we calculated the percentage of overlapping flooded areas relative to the total flood extent identified in ArcGIS:

Overlap Percentage = (Intersected Area/Total Flooded Area

in Benchmark) × 100[41]

This was quantified using metrics Intersection over Union (IoU) and total area difference, which provided a clear indication of each method's detection accuracy:

$$\text{IoU} = \text{Area of Intersection/Area of Union}\ [42]$$

$$\text{Area Difference} = |\text{AreaMap}_1 - \text{AreaMap}_2|$$

In addition, we calculated the commission and omission errors for each dataset, giving insight into false positives (non-flooded areas detected as flooded) and false negatives (flooded areas not detected):

$$\text{Commission Error (\%)} = (\text{FP}/(\text{TP} + \text{FP})) \times 100$$

$$\text{Omission Error (\%)} = (\text{FN}/(\text{TP} + \text{FN})) \times 100\ [43]$$

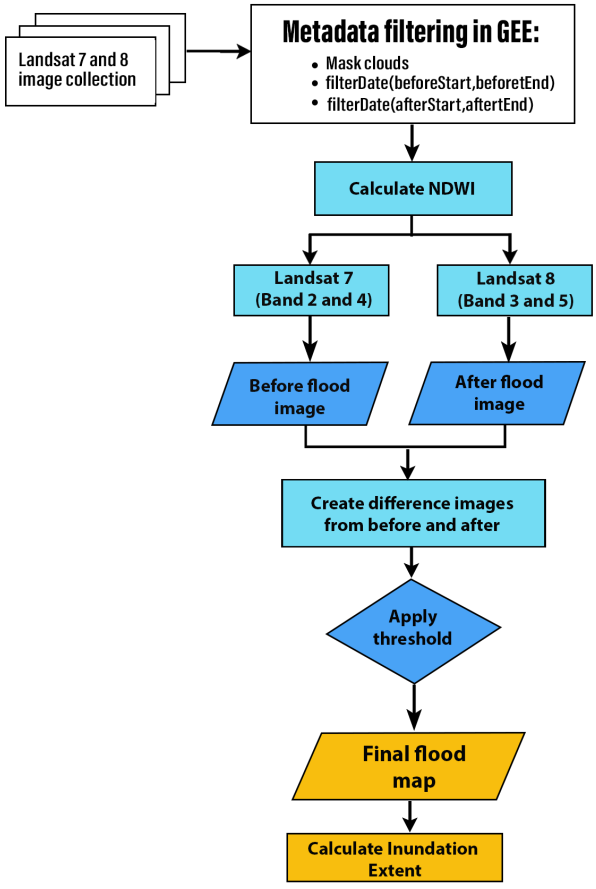

Figure 14. Flowchart of the proposed methodology for flood mapping using Landsat and GEE.

4. Results

In order to visually compare the extent of flooding, resulting flood maps based on Sentinel-1, Sentinel-2, and Landsat images for the Tetouan area in January 2021 are presented in **Figure 15**.

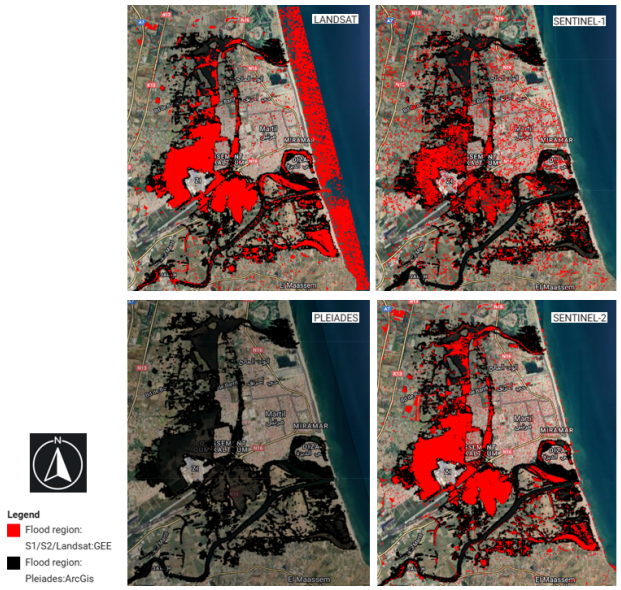

Figure 15. Flood maps generated by the presented methodologies based on Sentinel-1, Sentinel-2, and Landsat images for the Tetouan area.

The flood extent maps obtained were compared and evaluated. The result of the three methods using a thresholding approach, based on the VH band difference between Sentinel-1 images before and after the flood and on the NDWI difference of the study area generated by the Sentinel-2 and Landsat images is presented in **Figure 15**, where the flooded area appears in red and the permanent water appears in blue. The total extent of flooding was estimated at 891 hectares for Sentinel-1, 814 hectares for Sentinel-2, and 1237 hectares for Landsat which gave flooded hectare values close to the value obtained by the analysis performed with ArcGIS as shown in **Table 4**.

The following **Table 5** presents a comprehensive comparison of flood mapping metrics for Sentinel-2, Sentinel-1, and Landsat, using the ArcGIS flood map as a benchmark with an estimated flood area of 900 hectares. Key metrics—including flooded area, area difference, Intersection over Union (IoU), overlap percentage, commission error, and omission error—highlight each dataset's performance in capturing flood extent and alignment with the benchmark. These metrics provide a detailed view of each method's accuracy, precision, and potential limitations in flood detection.

Table 4. Hectares of inundated area using a thresholding approach.

Hectares of Area Studied	Hectares of ermanent Water	Hectares of Inundated Area with ArcGIS Analysis	Hectares of Inundated Area Using a Thresholding Approach		
			Sentinel-1	Sentinel-2	Landsat
5067	165	900	891	814	1,237

Table 5. Flood mapping performance metrics for Sentinel-2, Sentinel-1, and Landsat compared to ArcGIS benchmark.

Dataset	Flooded Area (ha)	Area Difference (ha)	IoU	Overlap Percentage (%)	Commission Error (%)	Omission Error (%)
Sentinel-2	814	86	0.4377	57.26	34.99	42.74
Sentinel-1	891	9	0.2181	35.05	63.41	64.95
Landsat	1,237	337	0.3347	58.95	56.35	41.05

5. Discussion

5.1. Comparison of Results

The quantitative comparison between Sentinel-2, Sentinel-1, and Landsat datasets against the ArcGIS benchmark (900 hectares) reveals distinct performance characteristics for each method in detecting flood extents.

Sentinel-2 detected a total flooded area of 814 hectares, resulting in an area difference of 86 hectares compared to the benchmark. With an Intersection over Union (IoU) of 0.4377 and an overlap percentage of 57.26%, Sentinel-2 provides moderate spatial accuracy, capturing a significant portion of the flooded regions. The commission error of 34.99% and omission error of 42.74% suggest that while Sentinel-2 accurately identifies many flooded areas, some discrepancies exist in alignment with the benchmark, potentially due to cloud cover and water misclassification in optical imagery.

Sentinel-1 estimated 891 hectares of flooded area, with a minimal area difference of 9 hectares relative to the benchmark, indicating strong agreement in total flooded area. However, the IoU of 0.2181 and a lower overlap percentage of 35.05% reflect limited spatial alignment with the benchmark, likely stemming from radar limitations in differentiating water from similar surfaces. The high commission error of 63.41% and omission error of 64.95% imply that while Sentinel-1's radar capabilities are beneficial under cloudy conditions, this method might overestimate or miss specific flood regions in more heterogeneous landscapes.

Landsat detected the highest flooded area at 1237 hectares, resulting in an area difference of 337 hectares compared to the benchmark, suggesting potential over-detection. With an IoU of 0.3347 and the highest overlap percentage at 58.95%, Landsat aligns moderately with the benchmark in flood spatial extent but shows a commission error of 56.35% and an omission error of 41.05%. These values indicate Landsat's ability to capture extensive flood areas effectively but with a tendency toward overestimation, particularly in large-scale flood events.

These metrics underscore the individual strengths and limitations of each dataset in flood mapping, with Sentinel-2 providing balanced spatial accuracy, Sentinel-1 achieving close area approximation under variable weather, and Landsat offering extensive coverage at the cost of slight over-detection.

5.2. Methodological Strengths

While real-time flood monitoring plays a crucial role in rescue operations, flood maps also play an important role in decision-making, planning, and implementing flood management options. The choice of algorithm depends on its implementation complexity and accuracy. For our study, we used three recently developed flood detection methods for the following reasons:

- They are simple to implement and effective for rapid real-time flood mapping.
- They can be easily extended to other regions with minimal required modifications.
- They have the potential for automated flood mapping.
- They utilize multi-source and publicly accessible datasets: Sentinel-1, Sentinel-2, and Landsat for result comparison and accuracy enhancement.
- They can be used with little or no experience in GIS or coding.

Thus, the methods proposed in this work were compared, leading to the following findings:

- Too often, limited technical expertise deprives the disaster-

stricken community of needed information. This practice provided near real-time, cloud-based, easy-to-use flood extent mapping methods designed to overcome technical limitations.

- Implementing our algorithm on GEE offers several advantages over conventional flood mapping and monitoring methods. The GEE platform hosts all available Sentinel-1, Sentinel-2, and Landsat images at petabyte scale and provides high-performance parallel computing facilities, offering researchers a unique opportunity to quickly access ready-to-analyze data necessary for flood monitoring and disaster management.
- Cloud processing on the GEE platform enables the use of auxiliary datasets to delineate flood extent (e.g., slope).
- By inputting the provided code and simply delineating the region of interest along with dates before and after, this methodology produces in seconds what a GIS user may take hours to accomplish.
- The user has various methodologies for creating flood maps depending on the availability of Sentinel-1, Sentinel-2, and Landsat images in their study area.

5.3. Uncertainty Analysis

All available Sentinel-1, Sentinel-2, and Landsat images were useful for rapid large-scale flood mapping and monitoring at the study area level. However, uncertainties exist in the generated flood maps.

The uncertainty of flood extent maps could arise from the low temporal resolution limited by the satellite revisit period of Sentinel-1 (6 to 12 days), Sentinel-2 (5 days), and Landsat 7 and 8 (16 days). Since floodwaters change rapidly, this temporal resolution may not be sufficient to track flood progression. This situation is exacerbated when considering a vast area.

Uncertainty arises in flood-prone areas based on SAR due to environmental conditions in the studied regions, such as wind presence at the time of image acquisition, topography, vegetation types, and built-up areas. All of these factors could influence results to some extent [44].

Flood-prone areas depended on the choice of threshold values, and the choice of these values may lead to underestimation or overestimation of the floodplain. Although threshold values were selected based on suggested and experimented values, they may limit the ability to detect all flooded locations.

Although active SAR images are less affected by clouds, in terms of captured surface information, they are not as rich as passive optical images at the same resolution [45].

Finally, seasonal variations in land cover and differences in acquisition parameters of Sentinel-1, Sentinel-2, and Landsat could result in differences in acquired images for water areas at the same location and over varying periods. Thus, using data from all three satellites will allow differentiation and comparison of individual events influencing floods. Additionally, to overcome these uncertainties, local knowledge is crucial.

5.4. Limitations and Potential Improvements

Despite the strengths of our methodology and the GEE platform in near real-time flood monitoring, we encountered a few limitations:

- We only used Sentinel-1 VH polarization data for flood mapping as they yielded better results compared to VV polarization in the thresholding method. We will actively explore the possibility of combining multiple polarization bands to improve flood mapping accuracy in the future.
- Optical methods suffer from cloud contamination and dense vegetation, hindering their application, especially in tropical regions. However, the flood map based on Sentinel-2 and Landsat could underestimate the floodplain due to lack of data induced by cloud cover during rainy flood periods.
- Floods are highly dynamic phenomena, and daily information is often required for effective disaster response. The operational revisit intervals of Sentinel-1 (6 to 12 days), Sentinel-2 (5 days), and Landsat 7 and 8 (16 days) are thus not sufficient for accurately tracking flood progression over time [12]. This revisit time means that images are not always available for a given area.
- A Google Earth Engine account is required to use the code developed in this study. The account may take a few days to become active.
- Storage space must be available on Google Drive (20 MB to 1 GB, depending on the study area size).
- A stable internet connection is required as processing is done on a cloud-based platform, and results are run through GEE JavaScript code.

5.5. Synthesis

The methods developed for mapping flooded areas seem to have satisfactory results and could be applied to flood risk management, as well as emergency situations. Thus, to summarize the results of this comparison, **Table 6** represents the strengths and weaknesses of methodologies based on Sentinel-1, Sentinel-2, and Landsat data.

Table 6. The strengths and weaknesses of methodologies based on Sentinel-1, Sentinel-2, and Landsat data.

		Sentinel-1	**Sentinel-2**	**Landsat 7 and 8**
Characteristics of the sensor affecting flood mapping	Frequency of revisit	6 to 12 days	5 days	16 days
	Spatial resolution	10 m × 10 m	10 m × 10 m	30 m × 30 m
	Imagery type	Synthetic Aperture Radar (SAR)	Multispectral optics	Multispectral optics
Availability and data processing on GEE	Image volume	Over 2.7 million images	Over 21.4 million images	• Over 2.7 million images for Landsat 7 • Over 1.7 million images for Landsat 8
	Start of image acquisition	October 3, 2014	November 29, 2015	April 30, 2013
	Access to images	Free	Free	Free
	Data processing	Python and JavaScript	Python and JavaScript	Python and JavaScript
Benefits		• High spatial resolution • Independent of weather conditions (cloud penetration) • Day and night imaging capability • Ability to penetrate vegetation • Close match to benchmark flood area (891 ha, 9 ha difference) • Consistent detection with lower area difference, showing reliability in flooded area estimation despite a lower overlap percentage (35.05%) and IoU (0.2181)	• High spatial resolution • Wide range of spectral bands • Easy to interpret • High revisit frequency (5 days) • Relatively high overlap percentage (57.26%) and IoU (0.4377), indicating good spatial agreement with benchmark • Balanced performance with moderate commission (34.99%) and omission errors (42.74%)	• Extensive archive of historical imagery (since 1972) • Large spatial and temporal coverage, suitable for monitoring floods over large regions and longer periods • Captures larger areas of flooding (1237 ha) but overestimates compared to benchmark • High overlap percentage (58.95%) and moderate IoU (0.3347), useful for extensive flood coverage
Disadvantages		• Less precise than optical imagery • More challenging to interpret due to lower IoU (0.2181) and high omission error (64.95%) • Significant commission error (63.41%) suggests overestimation in certain conditions	• Cannot observe through clouds or at night, limiting continuous monitoring • Shows moderate omission error (42.74%), missing some flooded areas • Small area difference (86 ha) indicates relative accuracy but still lower than Sentinel-1 in terms of flood area estimation	• Lower spatial resolution affects fine-scale flood detection • Longer revisit frequency limits rapid monitoring • Sensitive to weather conditions, similar to Sentinel-2, affected by cloud cover • High commission error (56.35%) and large area difference (337 ha) indicate significant overestimation of flooded areas

6. Conclusions

Flood management poses a challenging task due to its inevitable nature, complexity, and magnitude. Rapid extraction of flood areas has long been a focus of global researchers in water remote sensing. Recent floods were assessed in this study using a thresholding approach based on the difference in the VH band between Sentinel-1 images before and after flooding, as well as the NDWI difference of the study area generated by Sentinel-2 and Landsat images. The reliability of implementing these methodologies was further verified using the results of the analysis performed by ArcGIS in the same area.

The study presented flood mapping techniques using

Sentinel-1, Sentinel-2, and Landsat in Google Earth Engine (GEE). The study results showed that:

1. The presented methodologies significantly reduce the time for image selection and preprocessing by integrating the workflow within the cloud-based GEE platform, thereby achieving rapid and accurate flood area extraction.
2. Quantitative Performance and Recommendations:
    - Sentinel-1: This SAR-based method achieved a high spatial accuracy and weather-independent imaging capability, making it effective for real-time flood mapping in cloudy regions. The flood area estimation showed a close match with the benchmark data (891 ha compared to 900 ha, with only a 9 ha difference), although it had a relatively lower overlap percentage (35.05%) and higher omission error (64.95%), which suggests some areas of flooding may be missed. Recommendation: Sentinel-1 is highly suited for emergency monitoring, especially in areas with frequent cloud cover, due to its all-weather imaging capability. It is recommended for quick assessments when optical data may be limited.
    - Sentinel-2: This optical sensor provided a strong balance between spatial resolution and frequency, with an estimated flood area of 814 ha and an overlap percentage of 57.26%. Its omission error was moderate (42.74%), making it effective for moderately accurate flood detection. Sentinel-2's 5-day revisit frequency and higher spatial resolution also make it suitable for detailed flood mapping in cloud-free conditions. Recommendation: Sentinel-2 is recommended for areas requiring high spatial detail and moderate revisit frequency, ideally in cloud-free conditions. It is particularly valuable for mapping smaller, precise flood zones.
    - Landsat: Landsat provided the largest flood area estimation (1237 ha), but this included an overestimation compared to the benchmark, resulting in a high commission error (56.35%) and a significant area difference (337 ha). However, its extensive historical archive and large-scale spatial coverage make it suitable for longitudinal flood assessments over wide areas. Recommendation: Landsat is recommended for historical and large-scale flood analysis where long-term trends are necessary. Its 16-day revisit frequency makes it less ideal for real-time monitoring but useful for retrospective studies and large regional assessments.
    - Google Earth Engine has proven to be an efficient platform for large-scale flood mapping, allowing for automated processing and rapid analysis across different datasets. Its cloud-based infrastructure enables researchers and practitioners to overcome hardware limitations, making it highly suitable for processing large amounts of satellite data for flood analysis.

The methods developed for mapping flooded areas appear to yield satisfactory results and could be applied to flood risk management and emergency situations. The resulting map would further assist decision-makers in defining technical and regulatory steps and guidelines for potential anticipatory actions, better land use planning, and flood risk management. However, since this methodology is intended for global use and involves inherent uncertainties discussed in more detail in the preceding section, it is important that this tool not be used as the sole source of information for planning rescue interventions.

In conclusion, the use of satellite data available on the Google Earth Engine platform holds great potential for improving the accuracy and efficiency of flood mapping. This study has contributed to advancing research in this field and providing useful information for flood risk management. Further research is recommended to refine flood mapping techniques and address the limitations observed in each method, enhancing the overall robustness and applicability of remote sensing for flood management worldwide.

Author Contributions

All authors contributed to the study conception and design. Material preparation, data collection and analysis were performed by Y.L. (Yassine Loukili), Y.L. (Younes Lakhrissi) and S.E.B.A. The first draft of the manuscript was written by Y.L. (Yassine Loukili) and all authors commented on previous versions of the manuscript. All authors read and approved the final manuscript.

Funding

The authors declare that no funds, grants, or other support were received during the preparation of this manuscript.

Institutional Review Board Statement

The study does not require ethical approval.

Informed Consent Statement

Not applicable.

Data Availability Statement

Software required: Google Earth Engine, ArcGIS Pro.

The source codes are available for downloading at the link: Thesourcecodesareavailablefordownloadingatthelink: https://github.com/yslk327/FLOOD_MAPPING_GEE.

Acknowledgments

This research was made possible by the Intelligent Systems, Georesources and Renewable Energies Laboratory of Sidi Mohamed Ben Abdellah University of Fez. Thank you to professors Younes Lakhrissi and Safae Elhaj Ben Ali for assisting the lead author in the realization of this work.

Conflicts of Interest

The authors declare no conflicts of interest.

References

[1] Carmen, F., Abate, N., Faridani, F., et al., 2021. Google earth engine as multi-sensor open-source tool for supporting the preservation of archaeological areas: The case study of flood and fire mapping in Metaponto, Italy. Sensors. 21(5), 1791.

[2] Li, J., Wang, J., Ye, H., 2021. Rapid flood mapping based on remote sensing cloud computing and Sentinel-1. Journal of Physics: Conference Series. 1952, 022051.

[3] Loukili, Y., Lakhrissi, Y., Ali, S.E.B., 2022. Geospatial big data platforms: A comprehensive review. KN-Journal of Cartography and Geographic Information. 72(4), 293−308.

[4] Khan, R., Gilani, H., 2021. Global drought monitoring with big geospatial datasets using Google Earth Engine. Environmental Science and Pollution Research. 28, 17244–17264. DOI: https://doi.org/10.1007/s11356-020-12023-0

[5] Tiwari, V., Kumar, V., Matin, M.A., et al., 2020. Flood inundation mapping-Kerala 2018; Harnessing the power of SAR, automatic threshold detection method and Google Earth Engine. PLoS One. 15(8), e0237324. DOI: https://doi.org/10.1371/journal.pone.0237324

[6] Gumma, M.K., Thenkabail, P.S., Teluguntla, P.G., et al., 2020. Agricultural cropland extent and areas of South Asia derived using Landsat satellite 30-m time-series big-data using random forest machine learning algorithms on the Google Earth Engine cloud. GI-Science & Remote Sensing. 57(3), 302–322. DOI: https://doi.org/10.1080/15481603.2019.1690780

[7] Matgen, P., Hostache, R., Schumann, G., et al., 2011. Towards an automated SAR-based flood monitoring system: Lessons learned from two case studies. Physics and Chemistry of the Earth, Parts A/B/C. 36(7–8), 241–252. DOI: https://doi.org/10.1016/j.pce.2010.12.009

[8] Twele, A., Cao, W., Plank, S., et al., 2016. Sentinel-1-based flood mapping: a fully automated processing chain. International Journal of Remote Sensing. 37(13), 2990–3004. DOI: https://doi.org/10.1080/01431161.2016.1192304

[9] Chini, M., Hostache, R., Giustarini, L., et al., 2017. A hierarchical split-based approach for parametric thresholding of SAR images: Flood inundation as a test case. IEEE Transactions on Geoscience and Remote Sensing. 55(12), 6975–6988. DOI: https://doi.org/10.1109/TGRS.2017.2737664

[10] Goffi, A., Stroppiana, D., Brivio, P.A., et al., 2020. Towards an automated approach to map flooded areas from Sentinel-2 MSI data and soft integration of water spectral features. International Journal of Applied Earth Observation and Geoinformation. 84, 101951.

[11] Uddin, K., Matin, M.A., Meyer, F.J., 2019. Operational flood mapping using multi-temporal Sentinel-1 SAR images: A case study from Bangladesh. Remote Sensing. 11(13), 1581.

[12] Devries, B., Huang, C., Armston, J., et al. 2020. Rapid and robust monitoring of flood events using Sentinel-1 and Landsat data on the Google Earth Engine. Remote Sensing of Environment. 240, 111664.

[13] Mehmood, H., Conway, C., Perera, D., 2021. Mapping of flood areas using landsat with google earth engine cloud platform. Atmosphere. 12(7), 866.

[14] Sustainable Development Goals (SDG), 2022. Tangier Tetouan Al Hoceima regional report. Report number 3, December 2022. (in French). Available from: https://www.hcp.ma/region-tanger/Les-Objectifs-de-Developpement-Durable-Rapport-Regional-de-Tanger-Tetouan-Al-Hoceima-Version-francaise_a652.html. (cited 5 November 2024).

[15] Karrouchi, M., Ouazzani, M., Touhami, M., et al., 2016. Mapping of flooding risk areas in the Tangier-Tetouan region: Case of Martil Watershed (Northern Morocco). International Journal of Innovation and Applied Studies.

14, 1019–1035.

[16] Surface Water Detected (SWD), Satellite on January 13, 2021 NE of Tetouan, Province of Tetouan & Prefecture of M'diq-Fnideq, Region of Tanger-Tétouan-Al Hoceïma, Morocco. Available from: https://unosat.org/products/3010 (cited 5 November 2024).

[17] El Gharbaoui, A., 1980. Earth and Man in the Tingitana Peninsula. Study on man and the natural environment in the Western Rif. Works of the Scientific Institute, geology and physical geography series, no. 15. [Geography Thesis]. (in French)

[18] Sentinel-1 Observation Scenario Archive (S1-OSA). Available from: https://sentinel.esa.int/en/web/sentinel/copernicus/sentinel-1/acquisition-plans/observation-scenario-archive (cited 5 November 2024).

[19] Torres, R., Snoeij, P., Geudtner, D., et al., 2012. GMES Sentinel-1 mission. Remote sensing of environment. 120, 9−24.

[20] Baghdadi, N., Bernier, M., Gauthier, R., et al., 2001. Evaluation of C-band SAR data for wetlands mapping. International Journal of Remote Sensing. 22(1), 71−88.

[21] Henry, J.-B., Chastanet, P., Fellah, K., et al., 2006. Envisat multi-polarized ASAR data for flood mapping. International Journal of Remote Sensing. 27(10), 1921−1929.

[22] Anusha, N., Bharathi, B., 2019. An overview on Change Detection and a Case Study Using Multitemporal Satellite Imagery. In Proceedings of the International Conference on Computational Intelligence in Data Science (ICCIDS); Chennai, India, 21−23 February 2019; pp. 1−6. DOI: https://doi.org/10.1109/ICCIDS.2019.8862160

[23] Psomiadis, E., 2016. Flash flood area mapping utilising SENTINEL-1 radar data. In Proceedings of the Earth Resources and Environmental Remote Sensing/GIS Applications VII. SPIE Remote Sensing; Edinburgh, UK, 18 October 2016. pp. 382−392.

[24] Sentinel-1 script. Available from: https://code.earthengine.google.com/1a3f0b3b7fb364d754794c370acec0c9?noload=true (cited 5 November 2024).

[25] GEE API, 2024. Sentinel-1 algorithms. Available from: https://developers.google.com/earth-engine/sentinel1 (cited 5 November 2024).

[26] Vanama, V.S.K., Mandal, D., Rao, Y.S., 2020. GEE4FLOOD: Rapid mapping of flood areas using temporal Sentinel-1 SAR images with Google Earth Engine cloud platform. Journal of Applied Remote Sensing. 14(3), 034505.

[27] Earth Engine Data Catalog Sentinel-2 (EEDC S-2). Available from: https://developers.google.com/earth-engine/datasets/catalog/sentinel-2 (cited 5 November 2024).

[28] Kumar, H., Karwariya, S., Kumar, R., 2022. Google earth engine-based identification of flood extent and flood-affected paddy rice fields using Sentinel-2 MSI and Sentinel-1 SAR data in Bihar state, India. Journal of the Indian Society of Remote Sensing. 50(5), 791−803.

[29] SentiWiki. Available from: https://sentiwiki.copernicus.eu/web/copernicus-programme (cited 5 November 2024).

[30] Sentinel-2 script. Available from: https://code.earthengine.google.com/94df97b38500a21433e7d66fd229b0a1?noload=true (cited 5 November 2024).

[31] Landsat mission. Available from: https://www.usgs.gov/landsat-missions/landsat-satellite-missions (cited 5 November 2024).

[32] Google Cloud Landsat data (GCLD). Available from: https://cloud.google.com/storage/docs/public-datasets/landsat (cited 5 November 2024).

[33] Landsat script. Available from: https://code.earthengine.google.com/2fbf0a6ece18bbfd80e2eb11ab810b7b?noload=true (cited 5 November 2024).

[34] Earth Engine Data Catalog Sentinel-1 (EEDC-S1). Available from: https://developers.google.com/earth-engine/datasets/catalog/COPERNICUS_S1_GRD (cited 5 November 2024).

[35] Lee, J.-S., Jurkevich, L., Dewaele, P., et al., 1994. Speckle filtering of synthetic aperture radar images: A review. Remote Sensing Reviews. 8(4), 313−340.

[36] Abramov, S., Rubel, O., Lukin, V., et al., 2017. Speckle reducing for Sentinel-1 SAR data. In Proceedings of the 2017 IEEE International Geoscience and Remote Sensing Symposium (IGARSS); Fort Worth, TX, USA, 23-28 July 2017. pp. 2353−2356, DOI: https://doi.org/10.1109/IGARSS.2017.8127463

[37] Copernicus Global Land-Cover Layers (CGL-CL). Available from: https://developers.google.com/earth-engine/datasets/catalog/COPERNICUS_Landcover_100m_Proba-V-C3_Global. (cited 5 November 2024).

[38] Main-Knorn, M., Pflug, B., Louis, J., et al., 2017. Sen2Cor for sentinel-2. In Proceedings of the Image and Signal Processing for Remote Sensing XXIII. SPIE Remote Sensing, Warsaw, Poland. Volume 10427, pp. 37−48.

[39] Du, Y., Zhang, Y., Ling, F., et al., 2016. Water bodies' mapping from Sentinel-2 imagery with modified normalized difference water index at 10-m spatial resolution produced by sharpening the SWIR band. Remote Sensing. 8(4), 354.

[40] Li, W., Du, Z., Ling, F., et al., 2013. A comparison of land surface water mapping using the normalized difference water index from TM, ETM+ and ALI. Remote Sensing. 5(11), 5530−5549.

[41] Ortiz, A., Oliver, G., 2006. On the use of the overlapping area matrix for image segmentation evaluation: A survey and new performance measures. Pat-

tern Recognition Letters. 27(16), 1916−1926. DOI: https://doi.org/10.1016/j.patrec.2006.05.002

[42] Van Beers, F., 2018. Using intersection over union loss to improve binary image segmentation [Bachelor's thesis]. University of Groningen: Groningen, The Netherlands.

[43] Boschetti, L., Flasse, S.P., Brivio, P.A., 2004. Analysis of the conflict between omission and commission in low spatial resolution dichotomic thematic products: The Pareto Boundary. Remote Sensing of Environment. 91(3−4), 280−292. DOI: https://doi.org/10.1016/j.rse.2004.02.015

[44] Singha, M., Dong, J., Sarmah, S., et al., 2020. Identifying floods and flood-affected paddy rice fields in Bangladesh based on Sentinel-1 imagery and Google Earth Engine. ISPRS Journal of Photogrammetry and Remote Sensing. 166, 278−293.

[45] Chen, Z., Zhao, S., 2022. Automatic monitoring of surface water dynamics using Sentinel-1 and Sentinel-2 data with Google Earth Engine. International Journal of Applied Earth Observation and Geoinformation. 113, 103010.